

## PAPER

CrossMark  
click for updatesCite this: *RSC Adv.*, 2015, 5, 103760

## Adsorption of bovine serum albumin on superparamagnetic composite microspheres with a Fe<sub>3</sub>O<sub>4</sub>/SiO<sub>2</sub> core and mesoporous SiO<sub>2</sub> shell†

Xuemei Hou,<sup>a</sup> Hongbo Xu,<sup>a</sup> Lei Pan,<sup>a</sup> Yanlong Tian,<sup>b</sup> Xiang Zhang,<sup>b</sup> Lihua Ma,<sup>a</sup> Yao Li<sup>\*b</sup> and Jiupeng Zhao<sup>\*a</sup>

Magnetic sandwich structured mesoporous silica microspheres containing a silica-coated Fe<sub>3</sub>O<sub>4</sub> core and a layered mesoporous silica shell have been successfully synthesized by multi-step reactions. The as-prepared Fe<sub>3</sub>O<sub>4</sub>/SiO<sub>2</sub>/mesoporous SiO<sub>2</sub> (Fe<sub>3</sub>O<sub>4</sub>/SiO<sub>2</sub>/mSiO<sub>2</sub>) microspheres were characterized via X-ray diffractometry (XRD), transmission electron microscopy (TEM), nitrogen adsorption–desorption and vibrating sample magnetometry (VSM). The results indicate that these materials possess superior porosity with high surface areas and large pore volumes, while still maintaining the microspheres morphologies, which is beneficial for enrichment and purification applications. The microspheres were applied as adsorbents for bovine serum albumin (BSA). The adsorption equilibrium was well explained in the entire experimental region by the Langmuir isotherm model and the maximum adsorption amounts of BSA were calculated as high as 289 mg g<sup>-1</sup>. This work provides a promising approach for the design and synthesis of multifunctional microspheres, which can be used for potential applications in a variety of biomedical fields including drug delivery and biosensors.

Received 18th October 2015  
Accepted 24th November 2015

DOI: 10.1039/c5ra21773c

[www.rsc.org/advances](http://www.rsc.org/advances)

### 1. Introduction

Magnetic nanoparticles have attracted considerable attention in the past few decades due to their unique magnetic features and potential applications in biology and medicine.<sup>1–4</sup> In particular, superparamagnetic nanoparticles have proved to be very promising for biomedical applications, as they are not subject to strong magnetic interactions in dispersion.<sup>5–8</sup> Among these magnetic nanoparticles, superparamagnetic magnetite (Fe<sub>3</sub>O<sub>4</sub>) has been considered as an ideal candidate for these bio-related applications because of its good biocompatibility and stability in physiological conditions and low cytotoxicity.<sup>9–12</sup> Li *et al.*<sup>13</sup> reported a convenient synthesis of hydrophilic magnetite microspheres by a solvothermal reaction, but the resultant Fe<sub>3</sub>O<sub>4</sub> microspheres are ferromagnetic. Hyeon *et al.*<sup>14</sup> have synthesized a series of high-quality, monodispersed Fe<sub>3</sub>O<sub>4</sub> nanoparticles through thermal decomposition, not water dispersible. Therefore, biologically safe water-dispersible Fe<sub>3</sub>O<sub>4</sub> nanoparticles are needed.

Mesoporous silica with its large surface area and porosity, narrow pore size distribution, controlled morphology, and high thermal and hydrothermal stabilities has been extensively investigated due to their wide potential applications.<sup>15–18</sup> They are considered to be ideal protein and peptide hosts due to their high adsorption capacity, good dispersibility in aqueous solution, and good compatibility with the surrounding environment.<sup>19–22</sup> For many applications, mesoporous silica spheres with small particle sizes are advantageous from the view of adsorption equilibrium and kinetics. However, it is quite troublesome to separate small particles from a liquid. Therefore, magnetic particles have the advantage as they can be conveniently separated from an aqueous phase by applying an external magnetic field. Thus, a combination of porous materials and magnetic nanoparticles may be an effective media for separation and therefore has attracted wide attention in recent years.<sup>23</sup> In particular, magnetic core–shell nanocomposites composed of a Fe<sub>3</sub>O<sub>4</sub> core with superparamagnetism are expected to respond well to magnetic fields without any permanent magnetization. The silica shell is also of significance, because of its unique magnetic responsiveness, chemically modifiable surface, and has been widely used in bioseparation, drug delivery, magnetic resonance and diagnostic analysis.

Separation and purification of bio-products such as proteins, antibodies, amino acid, polysaccharides, and vitamins, are important tasks of bio-processing industries.<sup>24,25</sup> Bovine serum albumin (BSA), a globular blood plasma protein, is mainly used to stabilize enzymes. It is also used to determine the structures

<sup>a</sup>School of Chemical Engineering and Technology, Harbin Institute of Technology, Harbin, PR China. E-mail: [jiupengzhao@126.com](mailto:jiupengzhao@126.com); Fax: +86 0451 86403767; Tel: +86 0451 86403767

<sup>b</sup>Center for Composite Materials, Harbin Institute of Technology, Harbin, PR China. E-mail: [yaoli@hit.edu.cn](mailto:yaoli@hit.edu.cn); Fax: +86 0451 86403767; Tel: +86 0451 86403767

† Electronic supplementary information (ESI) available. See DOI: 10.1039/c5ra21773c

of other proteins, prevents the adhesive properties of enzymes and acts as a biosensor.<sup>26–28</sup> Recently, many efforts have been made to immobilize proteins on the surface of nanoparticles. Nanoparticles can, to a large extent, retain the bioactivity of proteins. Adalgisa Tavolaro *et al.*<sup>29</sup> have immobilized BSA on zeolite inorganic supports. Recently, Hee Moon *et al.*<sup>30</sup> reported the adsorption of BSA on monodispersed hollow silica nanospheres. Only limited work has been published on the application of magnetic mesoporous nanoparticles in the separation of proteins.

In this work, we reported the preparation of Fe<sub>3</sub>O<sub>4</sub>/SiO<sub>2</sub>/mSiO<sub>2</sub> core-shell composite nanoparticles, with the middle dense silica layer to protect the Fe<sub>3</sub>O<sub>4</sub> core from leaching under acidic conditions, while the outer porous silica layer exhibit a large surface area tunable pore size and larger surface. To the best of our knowledge, there is no such research on the building of a sandwich structure for the adsorption of molecular protein. The adsorption was carried out at different temperatures and pHs. Due to the inner magnetic core, the microspheres can be easily and rapidly separated from suspensions using an external magnetic field.

## 2. Experimental

### 2.1 Materials

Ferric chloride hexahydrate (FeCl<sub>3</sub>·6H<sub>2</sub>O), ethanol, ethylene glycol (EG), trisodium citrate (Na<sub>3</sub>Cit) and sodium acetate (NaOAc) anhydrous were purchased from Xilong Chemical Incorporated Company. Cetyltrimethylammonium bromide (CTAB), tetraethyl orthosilicate (TEOS), acetic acid (HAc) and sodium acetate (NaAc) were obtained from Recovery of Fine Chemical Industry Research Institute of Tianjin City. Bovine serum albumin (BSA) was purchased from Bodi Chemical Limited Liability Company. The water used was purified through a Millipore system. All chemicals were analytical grade and used without further purification.

### 2.2 Preparation of Fe<sub>3</sub>O<sub>4</sub> nanoparticles

The magnetic Fe<sub>3</sub>O<sub>4</sub> nanoparticles were synthesized according to a previous report with a slight modification.<sup>31</sup> In a typical process, 1.3 g of FeCl<sub>3</sub>·6H<sub>2</sub>O was dissolved in 40 mL EG to form a clear solution. Then 0.4 g of Na<sub>3</sub>Cit and 2.4 g of NaOAc were added under vigorous stirring. After vigorously stirring for 30 min, the resulting homogeneous dispersion was transferred into a Teflon-lined stainless-steel autoclave with a capacity of 80 mL, sealed, heated at 200 °C and maintained for 10 h. The as-prepared products were collected with a magnet and washed with ethanol and deionized water for several times, then dried at 60 °C under vacuum for further use.

### 2.3 Preparation of Fe<sub>3</sub>O<sub>4</sub>/SiO<sub>2</sub> nanoparticles

The synthesis of Fe<sub>3</sub>O<sub>4</sub>/SiO<sub>2</sub> nanoparticles were carried out by a modified sol-gel method.<sup>32</sup> Typically, 0.1 g as-prepared Fe<sub>3</sub>O<sub>4</sub> nanoparticles were treated with 0.1 M HCl aqueous solution (50 mL) by ultrasonication. After the treatment for 10 min, the magnetite particles were separated, washed with water, and

then homogeneously dispersed in the mixture of 40 mL ethanol and 10 mL deionized water by ultrasonication for about 10 min. Subsequently, 1 mL ammonia solution was added in the above solution under continuous mechanical stirring, and followed by 0.1 mL TEOS which was added dropwise. Finally, the reaction was allowed to proceed at room temperature for 6 h. The resulting products were washed with ethanol.

### 2.4 Preparation of Fe<sub>3</sub>O<sub>4</sub>/SiO<sub>2</sub>/mSiO<sub>2</sub> nanoparticles

The obtained Fe<sub>3</sub>O<sub>4</sub>/SiO<sub>2</sub> nanoparticles were redispersed in a mixed solution containing of CTAB (0.3 g, 0.82 mmol) deionized water (80 mL), concentrated ammonia aqueous solution (1.0 g, 28 wt%) and ethanol (60 mL). The mixed solution was homogenized for 0.5 h to form a uniform dispersion. 0.4 mL of TEOS (1.90 mmol) was added dropwisely to the dispersion with continuous stirring. After the reaction for 6 h, the product was collected with a magnet and washed repeatedly with ethanol and water to remove nonmagnetic by-products. Finally, the purified microspheres were redispersed in 60 mL of acetone and refluxed at 80 °C for 48 h to remove the template CTAB. The extraction was repeated three times, and the microspheres were washed with deionized water, and the Fe<sub>3</sub>O<sub>4</sub>/nSiO<sub>2</sub>/mSiO<sub>2</sub> microspheres were finally produced.

### 2.5 Adsorption experiments

Determination of the static adsorption capacities of BSA on the magnetic affinity beads was achieved by measuring the adsorption of BSA from the aqueous solution under different experimental conditions. 50 mg microspheres were added to a centrifuge tube containing 50 mL BSA solution with certain concentrations (varying from 100 to 400 mg L<sup>-1</sup>) and the centrifuge tube was shaken at 20, 30 and 40 °C for 24 h under pH = 4.7. After magnetic separation, the concentration of BSA in the supernatant solution was measured by a UV spectrophotometer at 280 nm detection wavelength. The amount of adsorbed BSA was calculated by using the following equation:

$$q_e = (C_0 - C)V/m$$

where  $q_e$  is the amount of BSA adsorbed affinity beads (mg g<sup>-1</sup>),  $C_0$  and  $C$  (mg L<sup>-1</sup>) are the initial and equilibrium concentrations of BSA, respectively.  $V$  is the volume of the aqueous solution (mL) and  $m$  is the weight of the affinity beads in the adsorption medium (g). For the recycling test, after adsorption process, protein-loaded composites were immersed in 20 mL of phosphate buffer solution (pH ~ 7.3) and shaken in an incubator at 200 rpm for 60 min. The composites were collected by magnetic separation. The regenerated composites were washed with water three times and dried at 60 °C under vacuum for reuse.

### 2.6 Characterization

Powder X-ray diffraction (XRD) patterns of the prepared products were carried out on a Dmax-rA powder diffractometer, Cu K $\alpha$  as a radiation source was used with an operating voltage of 40 kV and an operating current of 40 mA. Fourier transformed

infrared (FT-IR) spectra were recorded on a Bruker FT-IR spectrometer (VERTEX 70) with KBr pellets at room temperature. The morphologies and sizes of the as-prepared samples were characterized by Transmission Electron Microscopy (TEM, H-7650, Hitachi) with an accelerating voltage of 100 kV. Magnetic properties at room temperature were measured by a vibrating sample magnetometer (VSM, Lake Shore 7407) in a maximum field of 15 kOe. The protein concentration in the supernatant was analyzed by an UV-vis absorption spectrophotometer (Perkin Elmer, Lambda 950) at 280 nm.

### 3. Results and discussions

#### 3.1 Structure characterization of $\text{Fe}_3\text{O}_4/\text{SiO}_2/\text{mSiO}_2$ microspheres

The phase structures of the  $\text{Fe}_3\text{O}_4$ ,  $\text{Fe}_3\text{O}_4/\text{SiO}_2$ , and  $\text{Fe}_3\text{O}_4/\text{SiO}_2/\text{mSiO}_2$  microspheres were analyzed *via* XRD (Fig. 1). It can be seen in Fig. 1a that all the diffraction peaks are indexed to the face-centered cubic  $\text{Fe}_3\text{O}_4$  crystal structure (JCPDS card no. 19-0629) and no other peaks are detected. This indicates that the products are pure phase  $\text{Fe}_3\text{O}_4$ .<sup>31</sup> Fig. 1b displays a XRD pattern of the  $\text{Fe}_3\text{O}_4/\text{SiO}_2$  microspheres, which presents almost the same feature as that shown in Fig. 1a, and no diffraction peaks corresponding to  $\text{SiO}_2$  are observed because  $\text{SiO}_2$  is amorphous. In the case of the  $\text{Fe}_3\text{O}_4/\text{SiO}_2/\text{mSiO}_2$  microspheres, when the amount of coated  $\text{SiO}_2$  was increased, the intensities of all  $\text{Fe}_3\text{O}_4$  diffraction peaks decrease significantly. While the diffraction peak of  $\text{SiO}_2$  increased, there existed a broad peak at  $2\theta = 22^\circ$  which corresponded to the amorphous peak of  $\text{SiO}_2$ , which indicating that two silica shells have been coated on the surface of the  $\text{Fe}_3\text{O}_4$  microspheres.<sup>33</sup>

Fig. 2 shows typical TEM images of the  $\text{Fe}_3\text{O}_4$ ,  $\text{Fe}_3\text{O}_4/\text{SiO}_2$ , and  $\text{Fe}_3\text{O}_4/\text{SiO}_2/\text{mSiO}_2$  composite microspheres. As expected in Fig. 2a,  $\text{Fe}_3\text{O}_4$  microspheres are well dispersed and the average particle sizes ranged between 300 and 400 nm. From Fig. 2b, it can be observed that a typical core-shell structure has a dark core of  $\text{Fe}_3\text{O}_4$  and a less dark nonporous silica shell, implying that the  $\text{Fe}_3\text{O}_4$  nanoparticles have been successfully coated by a nonporous silica shell. The silica shell is about 10 nm in thickness. The particle size of  $\text{Fe}_3\text{O}_4/\text{SiO}_2/\text{mSiO}_2$  (Fig. 2c) is larger than that of the  $\text{Fe}_3\text{O}_4/\text{SiO}_2$  sample because of another

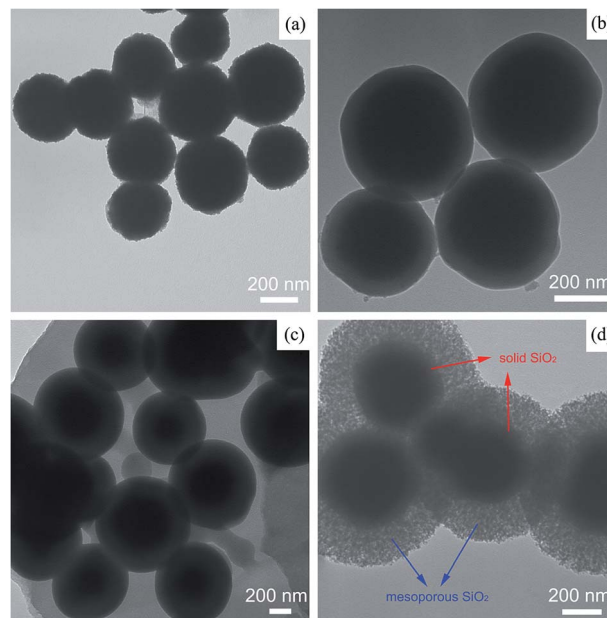


Fig. 2 TEM images of (a)  $\text{Fe}_3\text{O}_4$  and (b)  $\text{Fe}_3\text{O}_4/\text{SiO}_2$  (c)  $\text{Fe}_3\text{O}_4/\text{SiO}_2/\text{CTAB}/\text{SiO}_2$  and (d)  $\text{Fe}_3\text{O}_4/\text{SiO}_2/\text{mSiO}_2$  nanoparticles.

layer of  $\text{SiO}_2$ . Notably, the second layer  $\text{SiO}_2$  shell shows an evident mesoporous structure after treatment by acetone (Fig. 2d). The fabricated mesoporous structure not only offers a large number of exposed active sites because of high surface area, but also provides large accessible pore volume for the adsorption and release of large guest objects, thereby increasing the capability in adsorption and separation applications.

To further confirm the composition, the Fourier transform infrared (FT-IR) spectroscopy of the  $\text{Fe}_3\text{O}_4/\text{SiO}_2/\text{CTAB}/\text{SiO}_2$  and  $\text{Fe}_3\text{O}_4/\text{SiO}_2/\text{mSiO}_2$  composite were also investigated. Across the two samples, the wide peak at about 1600 and 3400  $\text{cm}^{-1}$  can be ascribed to the stretching and bending vibrations of the adsorbed water. The FT-IR spectra of  $\text{Fe}_3\text{O}_4$  nanoparticles obtained with  $\text{Na}_3\text{Cit}$  as an electrostatic stabilizer show absorption bands at 1611 and 1396  $\text{cm}^{-1}$  and are associated with a carboxylate group. Typical bands assigned to the Fe-O stretching are visible at around 580  $\text{cm}^{-1}$ . The absorption peaks

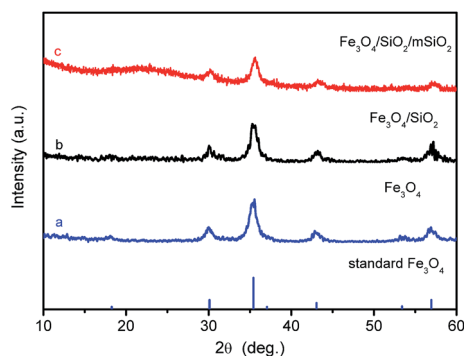


Fig. 1 XRD patterns of (a)  $\text{Fe}_3\text{O}_4$  and (b)  $\text{Fe}_3\text{O}_4/\text{SiO}_2$  and (c)  $\text{Fe}_3\text{O}_4/\text{SiO}_2/\text{mSiO}_2$  nanoparticles.

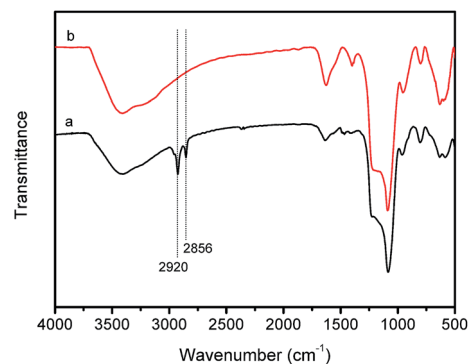


Fig. 3 FT-IR spectra of (a)  $\text{Fe}_3\text{O}_4/\text{SiO}_2/\text{CTAB}/\text{SiO}_2$  and (b)  $\text{Fe}_3\text{O}_4/\text{SiO}_2/\text{mSiO}_2$  nanoparticles.

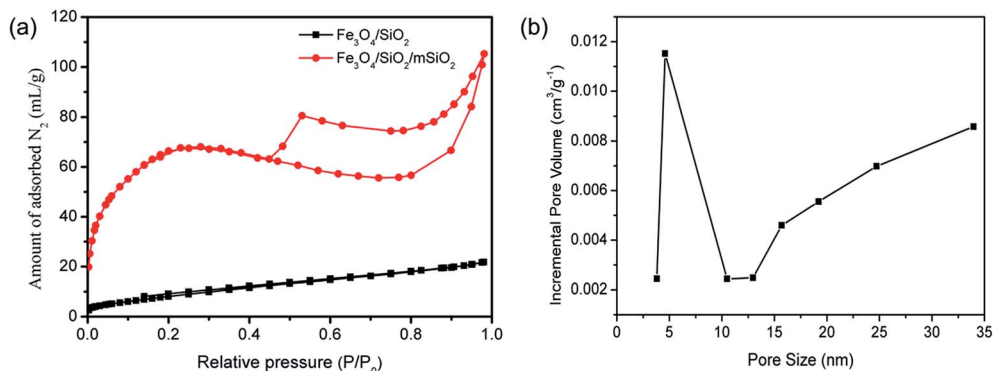


Fig. 4  $N_2$  sorption isotherms (a) and pore size distribution (b).

at 473, 796, 950 and  $1086\text{ cm}^{-1}$  are assigned to symmetric and asymmetric stretching vibrations of the framework and the Si–O–Si vibration, demonstrating that the  $Fe_3O_4$  was well encapsulated by the  $SiO_2$  layer. In Fig. 3a, the bands at around  $2920$  and  $2856\text{ cm}^{-1}$  can be assigned to CTAB and their disappeared in Fig. 3b, suggests that CTAB templates can be successfully removed by the extraction.<sup>32</sup>

The specific surface area and porosity of the  $Fe_3O_4/SiO_2/mSiO_2$  were determined by nitrogen sorption measurements. The obtained adsorption–desorption isotherms and BJH (Barratt–Joyner–Halenda) pore-size distribution curves are shown in Fig. 4. The isotherm can be classified as a type IV isotherm with a H3-type hysteresis loop at relative pressures ( $P/P_0$ ) between 0.4 and 1.0, indicating the typical characteristics of mesoporous materials.<sup>34</sup> The BET (Brunauer–Emmett–Teller) surface area of the magnetic mesoporous nanoparticles is calculated to be  $247\text{ m}^2\text{ g}^{-1}$  and the corresponding pore size distribution data calculated from the desorption branch of the nitrogen isotherm by the BJH method shows a narrow pore size distribution peaking at 4.6 nm.

Fig. 5a shows the magnetic hysteresis loops of the as-obtained  $Fe_3O_4$ ,  $Fe_3O_4/SiO_2$ , and  $Fe_3O_4/SiO_2/mSiO_2$  composite microspheres. The magnetic saturation ( $M_s$ ) values of the  $Fe_3O_4$ ,  $Fe_3O_4/SiO_2$ , and  $Fe_3O_4/SiO_2/mSiO_2$  microspheres are 77.5, 54.7, and  $18.3\text{ emu g}^{-1}$ , respectively. In addition, little

hysteresis, remanence and coercivity were detected for all of the samples. All of them show superparamagnetic behavior at room temperature. The small decrease of the  $M_s$  value of  $Fe_3O_4/SiO_2/mSiO_2$  microspheres compared to that of  $Fe_3O_4/SiO_2$  and  $Fe_3O_4$  microspheres can be attributed to the coated two layers of amorphous  $SiO_2$ . On placing a magnet beside the vial in Fig. 5b, the materials are quickly attracted to the side of the vial within a few seconds and the solution became transparent. Such an excellent magnetic property means that the  $Fe_3O_4/SiO_2/mSiO_2$  microspheres can be separated from the solution easily.

A probable formation mechanism of the resulting composite microspheres is also proposed as follows. First,  $Fe_3O_4$  nanoparticles were prepared using a solvothermal method by reduction of  $Fe(III)$  with EG in the presence of sodium acetate as an alkali source and biocompatible trisodium citrate ( $Na_3Cit$ ) as an electrostatic stabilizer. Because of the strong coordination between the  $Fe(III)$  ions and citrate groups, the surface of magnetite particles possess a layer of citrate groups and thus it favors the subsequent coating with silica. Then the as-prepared  $Fe_3O_4$  nanoparticles were coated with a  $SiO_2$  layer by a modified sol–gel process to obtaining  $Fe_3O_4/SiO_2$  nanoparticles with a uniform nonporous silica layer. Due to negative charge of hydroxy on the surface of the  $Fe_3O_4@SiO_2$  nanoparticles, the cationic surfactant CTAB could easily bond *via* an electrostatic interaction. As a result, the hydrolyzed silica precursor would

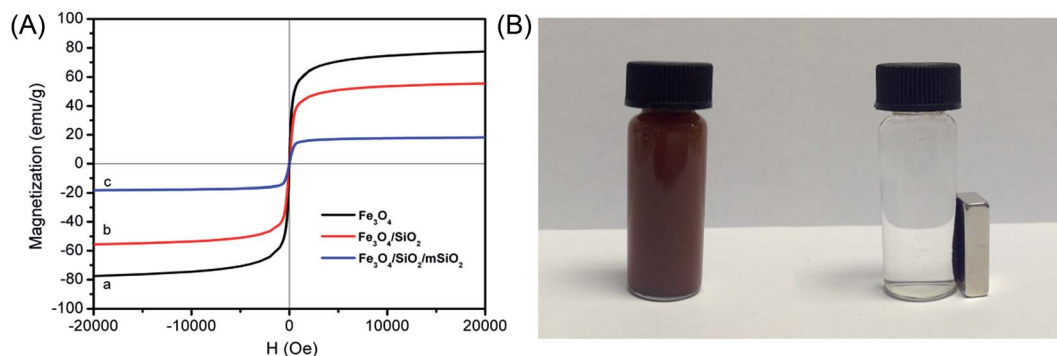


Fig. 5 (A) Magnetization curves of (a)  $Fe_3O_4$  and (b)  $Fe_3O_4@SiO_2$  nanoparticles and (c)  $Fe_3O_4/SiO_2/mSiO_2$  nanoparticles and (B)  $Fe_3O_4/SiO_2/mSiO_2$  nanoparticles were easily dispersed in water (left) and easy separation by magnet (right).

interact with the template CTAB through a self-assembly process under constant stirring to form the  $\text{Fe}_3\text{O}_4@\text{SiO}_2\text{-CTAB/SiO}_2$  nanocomposites. Finally, CTAB templates were removed in a mild way by acetone extraction and leaving an outer mesoporous  $\text{SiO}_2$  shell.

### 3.2 Adsorption isotherms

BSA was used as a model protein to study the adsorption behavior, which has a molecular diameter of about 4 nm.<sup>35</sup> The pH of the BSA solutions is an important parameter influencing the adsorption capacity onto adsorbents. Fig. 6 shows the effects of pH on the adsorption capacity of BSA on the  $\text{Fe}_3\text{O}_4/\text{SiO}_2/\text{mSiO}_2$  microspheres. The experiments were carried out with different pH of BSA solutions adjusted with HCl and NaOH solutions. It can be observed that the maximum adsorption capacity of  $\text{Fe}_3\text{O}_4/\text{SiO}_2/\text{mSiO}_2$  microspheres is at pH 4.7, which was the isoelectric point of BSA ( $\text{pI} = 4.7$ ). The amount of BSA adsorbed decreased significantly at pH values lower and higher than the pI of BSA. As is known, protein molecules at the pI are neutral, and the surface charge density of BSA molecules becomes almost zero. Furthermore, the  $\text{Fe}_3\text{O}_4/\text{SiO}_2/\text{mSiO}_2$  microspheres have a negative surface charge density due to the presence of surface hydroxyl groups. Thus, the  $\text{Fe}_3\text{O}_4/\text{SiO}_2/\text{mSiO}_2$  microspheres and BSA molecules were negatively and neutrally charged at the pI of BSA, respectively. Therefore, it is not surprising that BSA had a strong affinity for the  $\text{Fe}_3\text{O}_4/\text{SiO}_2/\text{mSiO}_2$  microspheres *via* electrostatic bonds at the pI of BSA.

In order to evaluate the efficiency of the prepared adsorbents, as-prepared  $\text{Fe}_3\text{O}_4/\text{SiO}_2/\text{mSiO}_2$  microspheres were employed to adsorb BSA molecules. An adsorption isotherm describes the relationship between the amount of adsorbate taken up by the adsorbent ( $q_e$ ) and the adsorbate concentration ( $C_e$ ) remaining in the solution after the system has attained equilibrium. The adsorption isotherms of BSA were carried out at pH = 4.7 and at different temperatures ( $T = 20, 30, 40^\circ\text{C}$ ), as shown in Fig. 7. The  $\text{Fe}_3\text{O}_4/\text{SiO}_2/\text{mSiO}_2$  microspheres exhibited very strong adsorption affinity for BSA molecules, and all the isotherms show a sharp initial slope, clearly indicating that  $\text{Fe}_3\text{O}_4/\text{SiO}_2/\text{mSiO}_2$  microspheres acted as high efficacy

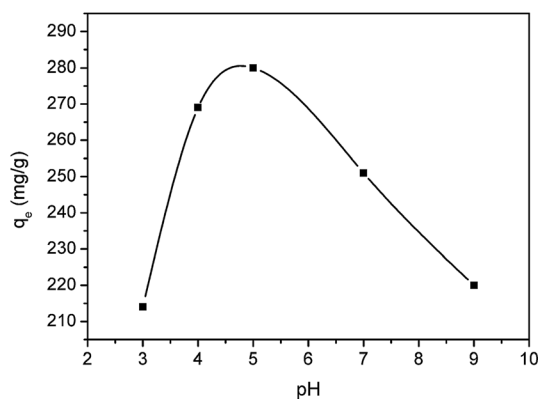


Fig. 6 The effect of pH on the BSA adsorption capacities of the nanoparticles at 30 °C.

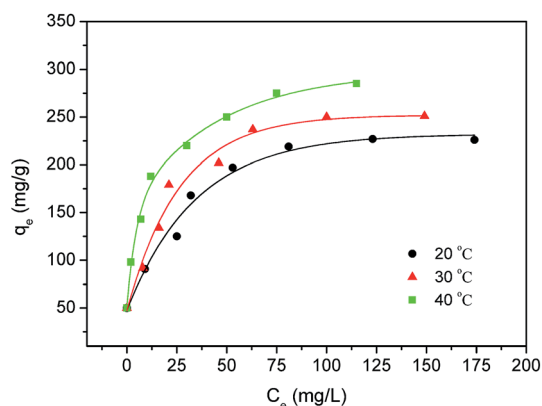


Fig. 7 The effects of temperature on the BSA adsorption capacities of the hollow composite nanoparticles.

adsorbents at a low BSA concentration. The adsorption equilibrium capacities are enhanced with the increasing of temperature, suggesting the endothermic process of the adsorption. Moreover, an increasing temperature is known to increase the diffusion rate of adsorbate molecules, due to the viscosity decrease of the solution, and this is also favorable for the adsorption process.

To further understand the adsorption mechanism, Langmuir and Freundlich adsorption models were used to test the adsorption process of the  $\text{Fe}_3\text{O}_4/\text{SiO}_2/\text{mSiO}_2$  microspheres. The Langmuir model is given as follows:

$$q_e = \frac{q_m K C_e}{1 + K C_e} \quad (1)$$

where  $q_e$  ( $\text{mg g}^{-1}$ ) and  $C_e$  ( $\text{mg mL}^{-1}$ ) are the adsorbed concentration and the equilibrium concentration of the adsorbate,  $q_m$  ( $\text{mg g}^{-1}$ ) is the maximum monolayer adsorption capacity, and  $K$  ( $\text{mL mg}^{-1}$ ) is the Langmuir constant. The linear form of the Langmuir isotherm is depicted by the following equation:

$$\frac{C_e}{q_e} = \frac{C_e}{q_m} + \frac{1}{K q_m} \quad (2)$$

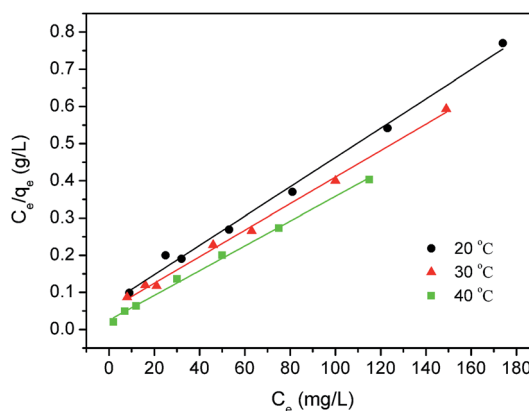


Fig. 8 Langmuir plots of the isotherms under different temperatures.

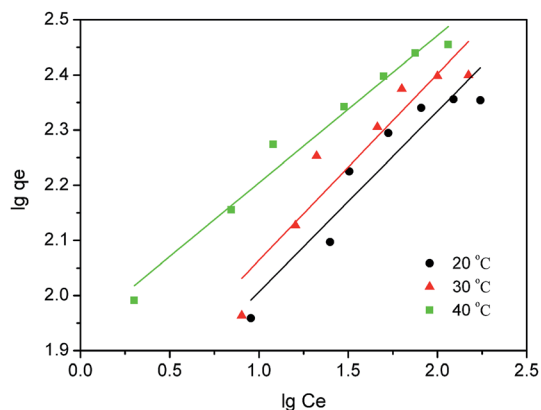


Fig. 9 Freundlich plots of the isotherms under different temperatures.

The Freundlich model, an empirical equation used to describe heterogeneous adsorption systems, can be expressed by:

$$\lg q_e = \lg K_f + \frac{1}{n} \lg C_e \quad (3)$$

where  $q_e$  is the solid-phase adsorbate concentration at equilibrium ( $\text{mg g}^{-1}$ ),  $C_e$  is the adsorbate concentration in the aqueous phase at equilibrium ( $\text{mg L}^{-1}$ ),  $n$  ( $\text{L g}^{-1}$ ) is the Freundlich parameter and  $K_f$  is the heterogeneity factor.

The adsorption isotherms of BSA followed the linearized Langmuir and Freundlich models and are shown in Fig. 8 and 9, respectively. The isotherm parameters were obtained and are summarized in Table 1. Based on the coefficient values determined as  $R^2$  for both isotherm models, the Langmuir isotherm model provided a better fit with the experimental data than the Freundlich isotherm model and the maximum Langmuir adsorption capacity of BSA is  $289 \text{ mg g}^{-1}$ . The applicability of the Langmuir isotherm suggests that the silica surfaces are energetically homogeneous for adsorbing BSA.

The adsorbent reusability is extremely important for reducing the cost of the practical applications process. The reusing property of composite microspheres for adsorption of BSA was also studied. For the release of BSA, protein-loaded composites were immersed in a phosphate buffer solution ( $\text{pH} \sim 7.3$ ). The results were presented in Fig. 10. It is clear to see that the microspheres have good renewable and reusable

Table 1 The correlated parameters for the adsorption of BSA according to Langmuir and Freundlich isotherm models<sup>a</sup>

Equation	Parameters	20 °C	30 °C	40 °C
Langmuir	$q_m$	253	289	300
	$K$	0.0574	0.0647	0.1320
	$R^2$	0.9931	0.9961	0.9963
Freundlich	$\lg K_f$	1.6791	1.7262	1.9376
	$n$	3.0525	2.9601	3.7469
	$R^2$	0.8885	0.8746	0.9695

<sup>a</sup>  $K$ , Langmuir constant;  $q_m$  ( $\text{mg g}^{-1}$ ), the maximum monolayer adsorption capacity.

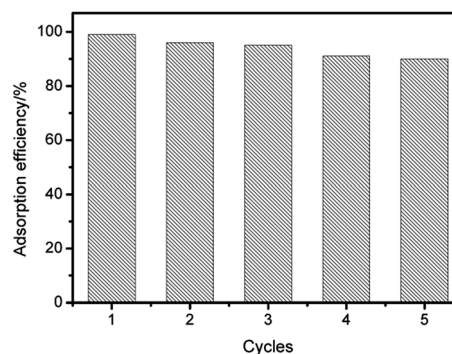


Fig. 10 Recyclability of  $\text{Fe}_3\text{O}_4/\text{SiO}_2/\text{mSiO}_2$  nanoparticles for absorbing BSA from aqueous solution.

property when repeated five times. The adsorption efficiency decreased slightly and yet still maintained 91% after being used five times.

The outer mesoporous silica shell thicknesses could be easily adjusted by the amount of TEOS. Fig. S1† shows that TEM micrographs of  $\text{Fe}_3\text{O}_4/\text{SiO}_2/\text{mSiO}_2$  composite microspheres with different shell thickness. The outer mesoporous silica shell thicknesses increased with an increase in the TEOS amount. The adsorption of protein on the different shell thicknesses of mesoporous silica are shown in Fig. S2.† It was noted that a thicker mesoporous silica shell led to a higher absorption performance. Upon the adsorption of BSA, the BSA adsorption rate was rapid during the initial stage, while the rate decreased over time until it reached equilibrium. These curves demonstrated the high number of fresh binding sites available for adsorption at the initial stage. However, it was difficult to occupy the remaining vacant binding sites over time due to the repulsive forces between the adsorbed molecules on the surface.

A comparison of BSA adsorption capacities on other materials reported in the literatures is summarized in Table 2. The value for adsorption capacity per weight is much higher than those reported for other inorganic adsorbents such as  $\text{TiO}_2$ , sepiolite, and silica gel. These adsorption results suggest that the magnetic mesoporous silica microspheres synthesized in this study can be an effective adsorption medium to absorb and separate other biomolecules.

Table 2 Comparison of the adsorption capacities of bovine serum albumin (BSA) on various adsorbents

Adsorbents	Experimental conditions			Adsorption capacities ( $\text{mg g}^{-1}$ )
	pH	Temperature	Concentration of BSA ( $\text{mg mL}^{-1}$ )	
$\text{TiO}_2$ (ref. 36)	5.0	30	10	82
Sepiolite <sup>37</sup>	7.0	25	1	219
Silica gel <sup>38</sup>	7.0	25	4.5	228
This work	4.7	30	1	285

## 4. Conclusions

In this paper, magnetic mesopores Fe<sub>3</sub>O<sub>4</sub>/SiO<sub>2</sub>/mSiO<sub>2</sub> microspheres were synthesized for the adsorption of BSA from aqueous solutions. The core-shell structure of the adsorbent formed by a magnetite wrapped with an inert silica layer provides ease of magnetic separation and protection from acid leaching in regeneration. The adsorbent could be easily separated from the solutions by using a magnet. The equilibrium results fitted the Langmuir isotherm model well in all experiments and the maximum adsorption capacity of BSA were calculated as 289 mg g<sup>-1</sup>. In conclusion, the Fe<sub>3</sub>O<sub>4</sub>/SiO<sub>2</sub>/mSiO<sub>2</sub> nanoparticles can be a potential candidate for the practical removal of other molecules from aqueous solutions.

## Acknowledgements

We thank National Natural Science Foundation of China (No. 51572058, 91216123, 51174063, 51502057), the Natural Science Foundation of Heilongjiang Province (E201436), the International Science & Technology Cooperation Program of China (2013DFR10630, 2015DFE52770) and Specialized Research Fund for the Doctoral Program of Higher Education (SRFDP 20132302110031).

## References

- 1 P. B. Shete, R. M. Patil, B. M. Tiwale and S. H. Pawar, *J. Magn. Mater.*, 2015, **377**, 406.
- 2 S. Singamaneni, V. N. Bliznyuk, C. Binek and E. Y. Tsybal, *J. Mater. Chem.*, 2011, **21**, 16819.
- 3 Y. Zhang and D. Zhou, *Expert Rev. Mol. Diagn.*, 2012, **12**, 565.
- 4 Y. Xu, A. Karmakar, D. Y. Wang, M. W. Mahmood, F. Watanabe, Y. B. Zhang, A. Fejleh, P. Fejleh, Z. R. Li, G. Kannarpady, S. Ali, A. R. Biris and A. S. Biris, *J. Phys. Chem. C*, 2010, **114**, 5020.
- 5 T. Li, X. Han, Y. L. Wang, F. Wang and D. L. Shi, *Colloids Surf., A*, 2015, **477**, 84.
- 6 D. V. Kurmude, A. B. Shinde, A. A. Pandit, C. M. Kale, D. R. Shengule and K. M. Jadhav, *J. Supercond. Novel Magn.*, 2015, **28**, 1759.
- 7 L. Zeng, L. Luo, Y. Pan, S. Luo, G. Lu and A. Wu, *Nanoscale*, 2015, **7**, 8946.
- 8 Z. G. Teng, X. D. Su, G. T. Chen, C. C. Tian, H. Li, L. Ai and G. M. Lu, *Colloids Surf., A*, 2012, **402**, 60.
- 9 F. Lan, Y. Wu, H. Hu, L. Xie and Z. Gu, *RSC Adv.*, 2013, **3**, 1557.
- 10 M. F. Shao, F. Y. Ning, J. W. Zhao, M. Wei, D. G. Evans and X. Duan, *J. Am. Chem. Soc.*, 2012, **134**, 1071.
- 11 L. H. Shen, J. F. Bao, D. Wang, Y. X. Wang, Z. W. Chen, L. Ren, X. Zhou, X. B. Ke, M. Chen and A. Q. Yang, *Nanoscale*, 2013, **5**, 2133.
- 12 R. Qiao, C. Yang and M. Gao, *J. Mater. Chem.*, 2009, **19**, 6274.
- 13 H. Deng, X. L. Li, Q. Peng, X. Wang, J. P. Chen and Y. D. Li, *Angew. Chem., Int. Ed.*, 2005, **44**, 2782.
- 14 J. Park, K. An, Y. Hwang, J. G. Park, H. J. Noh, J. Y. Kim, J. H. Park, N. M. Hwang and T. Hyeon, *Nat. Mater.*, 2004, **3**, 891.
- 15 Z. Teng, X. Su, Y. Zheng, J. Sun, G. Chen, C. Tian, J. Wang, H. Li, Y. Zhao and G. Lu, *Chem. Mater.*, 2013, **25**, 98.
- 16 J. Pizarro, X. Castillo, S. Jara, C. Ortiz, P. Navarro, H. Cid, H. Rioseco, D. Barros and N. Belzile, *Fuel*, 2015, **156**, 96.
- 17 T. Miyao, J. Tanaka, W. Shen, K. Hayashi, K. Higashiyama and M. Watanabe, *Catal. Today*, 2015, **251**, 81.
- 18 G. Yang, H. Gong, T. Liu, X. Sun, L. Cheng and Z. Liu, *Biomaterials*, 2015, **60**, 62.
- 19 J. Sivaguru, M. Selvaraj, S. Ravi, H. Park, C. W. Song, H. H. Chun and C. S. Ha, *J. Nanosci. Nanotechnol.*, 2015, **15**, 4784.
- 20 B. Faceto, E. Teixeira-Neto, H. O. Pastore, C. L. P. Oliveira and A. A. Teixeira-Neto, *Microporous Mesoporous Mater.*, 2015, **210**, 86.
- 21 S. Barma and B. Mandal, *Microporous Mesoporous Mater.*, 2015, **210**, 10.
- 22 A. G. M. da Silva, H. V. Fajardo, R. Balzer, L. F. D. Probst, A. S. P. Lovon, J. J. Lovon-Quintana, G. P. Valenca, W. H. Schreine and P. A. Robles-Dutenhefner, *J. Power Sources*, 2015, **285**, 460.
- 23 Y. Yang, Q. Wei, J. Zhang, Y. Xi, H. Yuan, C. Chen and X. Liu, *Biochem. Eng. J.*, 2015, **97**, 111.
- 24 J. Huang, R. Zhao, H. Wang, W. Q. Zhao and L. Y. Ding, *Biotechnol. Lett.*, 2010, **32**, 817.
- 25 P. Gagnon, *J. Chromatogr. A*, 2012, **1221**, 57.
- 26 K. Das and S. Kundu, *Colloids Surf., A*, 2015, **468**, 56.
- 27 X. Yan, J. Kong, C. Yang and G. Fu, *J. Colloid Interface Sci.*, 2015, **445**, 9.
- 28 M. Beragoui, C. Aguir, M. Khalfaoui, E. Enciso, M. Jose Torralvo, L. Duclaux, L. Reinert, M. Vayer and A. Ben Lamine, *J. Appl. Polym. Sci.*, 2015, **132**, 42055.
- 29 A. Tavoraro, P. Tavoraro and E. Drioli, *Colloids Surf., B*, 2007, **55**, 67.
- 30 M. J. Hwang, O. H. Kim, W. G. Shim and H. Moon, *Microporous Mesoporous Mater.*, 2013, **182**, 81.
- 31 J. Liu, Z. K. Sun, Y. H. Deng, Y. Zou, C. Y. Li, X. H. Guo, L. Q. Xiong, Y. Gao, F. Y. Li and D. Y. Zhao, *Angew. Chem., Int. Ed.*, 2009, **48**, 5875.
- 32 Y. Chi, Q. Yuan, Y. Li, J. Tu, L. Zhao, N. Li and X. Li, *J. Colloid Interface Sci.*, 2012, **383**, 96.
- 33 J. H. Wang, S. R. Zheng, Y. Shao, J. L. Liu, Z. Y. Xu and D. Q. Zhu, *J. Colloid Interface Sci.*, 2010, **293**, 349.
- 34 J. Hu, S. Huang, X. Huang, Z. Kang and N. Gan, *Microporous Mesoporous Mater.*, 2014, **180**, 197.
- 35 X. A. Diao, Y. J. Wang, J. Q. Zhao and S. L. Zhu, *Chin. J. Chem. Eng.*, 2010, **493**, 18.
- 36 C. E. Giacomelli, M. J. Avena and C. P. DePauli, *J. Colloid Interface Sci.*, 1997, **188**, 387.
- 37 M. Alkan, O. Demirbas, M. Dogan and O. Arslan, *Microporous Mesoporous Mater.*, 2006, **96**, 331.
- 38 C. E. Giacomelli and W. Norde, *J. Colloid Interface Sci.*, 2001, **233**, 234.